DENTAL MATERIALS XXX (2015) XXX.E1–XXX.E15

Available online at www.sciencedirect.com

ScienceDirect

journal homepage: www.intl.elsevierhealth.com/journals/dema

Periodontal-like gingival connective tissue attachment on titanium surface with nano-ordered spikes and pores created by alkali-heat treatment

Eiji Kato[a], *Kaoru Sakurai*[a], *Masahiro Yamada*[a,b,*]

[a] *Department of Removable Prosthodontics & Gerodontology, Tokyo Dental College, Tokyo, Japan*
[b] *Oral Health Science Center, Tokyo Dental College, Tokyo, Japan*

ARTICLE INFO

Article history:
Received 5 August 2014
Received in revised form
11 November 2014
Accepted 27 January 2015
Available online xxx

Keywords:
Fibroblasts
Gingival fiber
Nanotopography
Peri-implant tissue
Surface modification

ABSTRACT

Objectives. Establishment of periodontal-like connective tissue attachment is one of the outstanding issues in implant dentistry. Organized nanotopographic titanium surface may acquire periodontal-like connective tissue attachment with activation of fibroblastic function. This study aimed to evaluate gingival fibroblastic function and connective tissue attachment on two types of nanotopographic titanium surface created by alkali-heat (AH) treatment.

Methods. Commercially pure titanium turned discs with or without acid-etching or two types of AH treatment, underwent scanning electron microscopic evaluation in surface topography. Rat gingival fibroblasts cultured on the discs evaluated in terms of cellular adhesion, collagen synthesis and physicochemical binding strength of deposited collagen on the surfaces. Turned or the AH-treated pure titanium mini-implants were placed on the hard palatal plate of rabbits and underwent histological evaluation at 8 weeks postoperatively.

Results. Both AH-treated surfaces were characterized by numerous well-organized fine nanospikes with crevasses and nanoholes, and uniform shaggy-like nanotopography with a sponge-like inner network, respectively. These nanotopographic surfaces enhanced cellular adhesion and collagen synthesis and toughened binding strength of deposited collagen sufficiently to resist against experimental overloading and inflammatory conditions by inclusion of collagen fibers into the surface, as compared with turned or acid-etched surfaces. The AH-treated mini-implants yielded inclusion of gingival connective tissue into the nanotopographic surface structure, with collagen fiber directions mimicking periodontal tissue in the transmucosal area. These features were not seen on turned surface implants.

Significance. The well-organized nanotopographic titanium surface with nanospikes and pores by the AH treatment enhanced gingival fibroblastic collagen synthesis and acquired periodontal-like connective tissue attachment with substantial detachment resistance.

* *Corresponding author at*: Department of Removable Prosthodontics & Gerodontology, Tokyo Dental College, 2-9-18 Misaki-chou, Chiyoda-ku, Tokyo 101-0061, Japan. Tel.: +81 03 6380 9201; fax: +81 043 270 3935.
E-mail address: masayamada1020@gmail.com (M. Yamada).

http://dx.doi.org/10.1016/j.dental.2015.01.014
0109-5641/

1. Introduction

Titanium dental implant therapy is well-known as one of the prosthodontic treatment options available for morphological and occlusal reconstruction of the edentulous alveolar ridge. As well as sufficient osseointegration strength, firm soft tissue sealing at the transmucosal portion of the implant is also required for long-term clinical stability, to act as a biological barrier against the ingress of oral bacteria and preventing infection of the peri-implant tissue [1,2].

Biological sealing around periodontal gingival tissue is dependent not only on epithelial attachment but also on attachment of connective tissue to the root surface *via* dentogingival fibers. These consist of both gingival and Sharpey's fibers. Collagen fibrils with a diameter of approximately 70 nm gather into collagen fascicles with a few micrometers in diameter, and are inserted into cementum on the root surface as Sharpey's fibers. Gingival fibers are oriented perpendicularly to the root surface and subsequently extend occlusally and apically, terminating in connective tissue (dentogingival fibers) and the alveolar periosteum (dentoalveolar fibers). This Sharpey's fiber–gingival fiber complex anchors the connective tissue layer firmly to the tooth root and alveolar bone, and plays an important role in resistance against inflammation and mechanical stress on periodontal gingival tissue [3,4]. The same principle is also adopted for soft tissue sealing around peri-implant tissue. However, there is a critical difference between periodontal and peri-implant tissues. Certain microtopographical approaches with a microgrooved [5–7] or porous surface [8,9] attempted to make peri-implant tissue mimic periodontal tissue. However, the direct connection of gingival connective tissue with inclusion of collagen fibers, such as Sharpey's fibers, has not yet been established on an implant surface [1,10–12].

In this context, nanotopographical surface modification may be one of the solutions for the creation of Sharpey's fiber-like structures on a titanium surface. A biocompatible material surface with three-dimensional (3D) internal architecture, in conjunction with submicron superficial pores, may allow the inclusion of collagen fibers produced by fibroblasts into the internal structure [13]. Moreover, nanotopography can coexist with the microtopography of the substrate and synergistically influence cellular behavior on the surface [14–21]. Nanometer-sized protrusions can modulate cellular attachment, including the formation of focal adhesion plaques and cytoskeletal arrangement [22], and govern subsequent cellular proliferation and extracellular matrix (ECM) production [14,23]. For example, 3D monolithic scaffolds fabricated from carbon nanotubes with nanometer-sized spikes and pores on the surface entangled cellular projections of myoblasts or osteoblasts, and allowed cellular infiltration into the porous internal microstructure [24] and enhancement of cellular differentiation [25–27].

Alkali-heat (AH) treatment is the one of titanium surface modification methods to create nanotopography and involves treating the titanium surface by boiling in a sodium hydroxide solution followed by furnace-heating. This type of treatment has been reported to form a sodium titanate layer on the titanium surface through erosion of the superficial substrate [28–30]. In addition to the microgeometry of the titanium substrate, the concentration of the sodium hydroxide solution, boiling or heating temperature, and the duration of the process determines the final nanotopographical features. We have created well-organized numerous nanospikes with nanocrevasses and pores underlain by a 3D internal network on titanium surface by the modification of AH-treatment. It was hypothesized that such a nanofeatured titanium surface provided fibroblastic cells a niche to exert their inherent cellular function and to insert collagen fibers into the surface's internal structure. The purpose of this *in vitro* and *in vivo* study was to determine whether the nanofeatured titanium surface affected fibroblastic function and connectivity of deposited collagen with the titanium surface under various detachment treatment, with assessment of topographical, physicochemical and mechanical properties of the surfaces, and whether the nanofeatured titanium surface established the direct connection of gingival connective tissue with the inclusion and orientation of collagen fibers mimicking periodontal gingival connective tissue.

2. Materials and methods

2.1. Sample preparation

Commercially pure grade 2 turned titanium discs (20 mm diameter and 1 mm thickness) as a culture substrate, turned titanium mini-screws (0.5 mm diameter and 5.5 mm length) and grade 1 titanium film (10 mm^2 and 0.1 mm thickness) were purchased (Nishimura Co., Ltd., Fukui, Japan). The titanium samples were washed under ultrasonication with a series of ethanol and Milli-Q water after acetone cleaning. The acid-etched surface was prepared by immersion of the turned surface discs in 67% (w/w) sulfuric acid solution at 120 °C for 75 s [31]. Two types of nanotopographical titanium surfaces were prepared by two AH-treatment protocols. In previously reported protocol [32], the cleaned turned discs were boiled in 5 mol/L sodium hydroxide solution at 60 °C for 24 h. After being washed in Milli-Q water and air-dried, the discs were heated in a furnace with an increase in temperature at a rate of 5 °C/min and sintered at 600 °C for 1 h. After sintering, the discs were naturally cooled. In the other protocol (our modified protocol), the discs were boiled in 10 mol/L sodium hydroxide solution at 90 °C for 24 h, followed by the same subsequent process as previously described. All prepared samples were rinsed by ultrasonication in distilled water for 10 min, and stored in ambient conditions, in the dark, for 4 weeks prior to use. All of the discs and films for culture experimentation were placed on 12-well culture-grade polystyrene plates.

2.2. Surface characterization

The surface topography of the sample discs was evaluated by observation *via* scanning electron microscopy (SEM; XL30, Philips, Eindhoven, Netherlands) and the surface roughness measurements were evaluated using a 3D-measuring laser microscope (LEXT OLS4000, Olympus, Tokyo, Japan) with a cut-off value of 8 μm and a measurement length of 120 μm. The number and density of nanospikes on both types of

Please cite this article in press as: Kato E, et al. Periodontal-like gingival connective tissue attachment on titanium surface with nano-ordered spikes and pores created by alkali-heat treatment. Dent Mater (2015), http://dx.doi.org/10.1016/j.dental.2015.01.014

the nanotopographic surfaces were analyzed *via* SEM surface images using an image analyzer (ImageJ, National Institutes of Health, Bethesda, MD, USA). The thickness, porous structure and chemical composition of both types of AH-treated surfaces were evaluated by image analysis of SEM images and elemental analysis using an electron probe microanalyzer (EPMA, JXA-8200, JEOL Ltd., Tokyo, Japan) on cross-sectional specimens of AH-treated titanium films prepared by cutting the film with stainless steel scissors. Three areas were measured per sample, and the data were averaged. The set of measurements was performed in three independent samples.

2.3. Oral fibroblastic cell culture

Fibroblasts were obtained from the palatal tissue of 12-week-old Sprague-Dawley rats by reference to the methodology in previous article [33]. Briefly, the palatal gingiva was washed with 1% PBS and incubated in 0.1 units/ml collagenase/0.8 units/ml dispase solution for 60 min, followed by separating the connective tissue from the epithelial layer. Then, the connective tissue was dissected into small pieces (<1 mm^2) and digested in 0.25% collagenase for 12 h. The liberated cells were collected and plated in 100 mm plastic tissue culture dishes with Dulbecco's modified Eagle's medium supplemented with 10% fetal bovine serum and antibiotic–antimycotic solution, containing 100 U ml/L penicillin G sodium, 100 lg ml/L streptomycin sulfate and 250 ng ml/L amphotericin B in a humidified atmosphere of 95% air and 5% CO_2 at 37 °C. The cells were passaged for a second time when 80% confluency was achieved. After the second passage, the cells were detached using 0.25% Trypsin-1 mM EDTA-4Na and seeded directly onto the titanium discs or films with turned, 5 or 10 M AH-treated or acid-etched surfaces at 3.0×10^4 cells/cm^2. The medium was renewed every 3 days. This study protocol was approved by the Animal Research Committee of Tokyo Dental College (Protocol No. 232604).

2.4. Cellular morphology

On day 1, the culture of gingival fibroblasts on discs with turned, 5 or 10 M AH-treated or acid-etched surfaces, were fixed in 10% neutral buffered formalin for 30 min. The cells were treated with 0.1% Triton X for 5 min, and then stained with 2% rhodamine phalloidin (Actin filament red color, Molecular Probes, OR, USA) in PBS and the fluorescent dye 4′,6-diamidino-2-phenylindole (DAPI; Nuclei blue color, Vector, CA, USA) in a mounting agent. Cell morphology and cytoskeletal arrangement were observed under a fluorescent photomicroscope (Axiophoto2, Carl Zeiss Co., Ltd., Jena, Germany). Cell morphometry was analyzed using ImageJ software.

2.5. Cellular attachment and proliferation

The number of cells in the cultures from days 1 and 7 on discs with turned, 5 or 10 M AH-treated or acid-etched surfaces was evaluated by tetrazolium salt-based colorimetry (WST-1, Roche Diagnostics, Tokyo, Japan). Each culture was incubated at 37 °C for 4 h in 1 mL fresh culture media containing 100 μL of WST-1 reagent. The amount of formazan product produced by viable cells was measured by colorimetry at 420 nm using a microplate reader. The proliferative activity of cells was measured by bromodeoxyuridine (BrdU) incorporation during DNA synthesis. On day 4 of surface culture, a 100 mM BrdU solution (100 ml) (Roche Diagnostics, Tokyo, Japan) was added to the culture wells and incubated for 10 h. After denaturing DNA, the cultures were incubated with anti-BrdU antibody conjugated with peroxidase for 90 min and exposed to tetramethylbenzidine for color development. Absorbance was measured using an enzyme-linked immunosorbent assay reader at 370 nm.

2.6. Gene expression analysis

Gene expression was analyzed on days 7 and 14 using reverse-transcriptase polymerase chain reaction (PCR). The total RNA in these cultures was extracted using TRIzol (Invitrogen, Carlsbad, CA, USA) and a purification column (RNeasy, Qiagen, Valencia, CA, USA). Following DNAse I treatment, reverse transcription of 0.5 mg total RNA was performed using MMLV reverse transcriptase (Clontech, Carlsbad, CA, USA) in the presence of oligo(dT) primer (Clontech). PCR was performed using Taq DNA polymerase (EX Taq; Takara Bio, Madison, WI, USA) to detect collagen I and III mRNA using primer designs and the PCR condition established previously [34]. The forward and backward primers were designed: collagen I: 5′-GGCAACAGTCGATTCACC-3′ and 5′-AGGGCCAATGTCCATTCC-3′, collagen III: 5′-CCTGGACTCAGGGTATC-3′ and 5′-TGCAGGG-CCTGGACTACC-3′, respectively. The annealing temperature and the amplification cycles were set at 58 °C and 28 cycles for collagen I and 60 °C and 25 cycles for collagen III. The PCR products were visualized on 1.5% agarose gel by ethidium bromide staining. Band intensity was detected under UV light and normalized with reference to glyceraldehyde-3-phosphate dehydrogenase (GAPDH) mRNA. The gene expression analyses were performed three to five times and representative data sets presented after confirming consistency.

2.7. Collagen production

To quantify collagen production, on day 21, Sirius red staining-based colorimetric assay was employed for cultures on discs. Cultures from different groups were washed with pre-warmed PBS at 37 °C for 1 min and fixed with Bouin's fluid for 1 h at room temperature. The cultures were washed with ddH_2O and treated with 0.2% aqueous phosphomolybdic acid for 1 min. Then, the cultures were washed again with ddH_2O and stained with Sirius red dye (C.I. No. 35780, Pfaltz and Bauer, Stamford, CT, USA) dissolved in saturated aqueous picric acid (pH 2.0) at a concentration of 100 mg/100 ml for 90 min with mild shaking. The cultures were washed with 0.01 N hydrochloric acid for 2 min to remove all nonbound dye. Afterwards, 600 μl of 0.1 N sodium hydroxide was added to dissolve the staining using a microplate shaker for 30 min at room temperature. The optical density (OD) of the solution was then measured using a spectrophotometer at 550 nm against 0.1 N sodium hydroxide as a blank. The OD value on each culture was subtracted by the value on the corresponding disk without cells.

Please cite this article in press as: Kato E, et al. Periodontal-like gingival connective tissue attachment on titanium surface with nano-ordered spikes and pores created by alkali-heat treatment. Dent Mater (2015), http://dx.doi.org/10.1016/j.dental.2015.01.014

2.8. Analysis of deposition method of ECM on surface

For evaluation of surface morphology of ECM, on day 21, the cultures on discs with turned, 5 or 10 M AH-treated, and acid-etched surfaces underwent SEM observation after fixation with 2.5% glutaraldehyde and dehydration in a graded series of ethanol (50–100%). To determine inclusion of deposited ECM into the nanofeatured surface, day 21 cultures on titanium films with 5 or 10 M AH-treated surfaces were cut with stainless steel scissors after fixation with 2.5% glutaraldehyde and dehydration in a graded series of ethanol (50–100%). SEM observation with a bird's eye view and EPMA-based elemental determination on cross-sectional specimens of the film with the superficial culture layer was then undertaken.

2.9. Collagen detachment assay

For evaluation of the mechanical, enzymatic and chemical strengths of deposited collagen on each surface under overloading or inflammatory conditions, day 21 cultures on discs were subjected to ultrasonication or exposure to collagenase or hydrogen peroxide. The culture was then washed twice with PBS. Subsequently, the cultures in PBS were put on ultrasonic equipment (UT105, Sharp, Tokyo, Japan) at 100 W and 35 kHz for 1 min to simulate an overloading condition. To simulate an inflammatory condition, the remaining day 21 cultures were incubated at 37 °C in PBS containing 0.1 U/ml collagenase (Roche Diagnostics) for 1 h or 0.3 mmol/L hydrogen peroxide for 3 h, respectively. After detachment treatment, the cultures were stained with Sirius red and absorbance was measured according to the protocol described above. The OD value on each culture was subtracted by the value on the corresponding disk without cells. The percentage of remaining collagen was calculated as [(Sirius red absorbance of the culture after detachment treatment/the absorbance of the corresponding duplicated day 21 culture without detachment treatment) × 100] (%). In addition, following detachment treatment, some of the day 21 cultures underwent SEM observation after fixation with 2.5% glutaraldehyde and dehydration in a graded series of ethanol (50–100%) in order to evaluate the morphology of the mode of detachment.

For all culture experiments with quantitative assay except for cellular morphology, three independent cultures were evaluated in each group ($n = 3$) using different batch of the cells and there were at least three replicates in each experiment. To assess cellular morphometry, six single cells with typical morphological features were randomly selected from three different points on the titanium surface. The mean value of the seven single cells was set as a representative value for each sample. Each experiment was repeated five times with different discs and cell batches in each group ($n = 5$).

2.10. Animal surgery and histological observation

Sixteen-week-old male Japanese white rabbits weighing 3.0 – 3.5 kg (Fig. 5A) were used in this study. The rabbits were anesthetized by intramuscular administration of 2.5% thiopental sodium (Ravonal, Mitsubishi Tanabe Pharma Corporation, Osaka, Japan) prior to operation. Following local anesthetic administration of 2% lidocaine with 1:80,000 adrenaline (Xylocaine, Dentsply Sankin, Tokyo, Japan) into the palatal gingiva, the palatal gingival tissue was punched out at a distance of 2.0 mm from the central incisors and the underlying hard palatal plate was drilled for implantation holes using a round bur and stainless steel hand reamer. Titanium mini-screws (Fig. 5B) with turned (Fig. 5C–E) or 10 M AH-treated surfaces (Fig. 5F–H) were bilaterally placed into the hard palatal plate close to the upper central incisors, with the coronal portion of the implant threading running flush with the gingival tissue surface, and the gingival connective tissue contacting the submerged implant surface within 0.5 mm of the most coronal portion of implant threading (Fig. 5I). The animals were kept in separate cages for 8 weeks in order to ensure complete healing of peri-implant gingival tissue [35]. The experimental protocols were approved by the Animal Research Committee of Tokyo Dental College (Protocol No. 252602).

2.11. Histological and SEM observation of connective tissue attachment on implants

After 8 weeks of healing, the animals were sacrificed with an intravascular overdose of 2.5% thiopental sodium (Ravonal, Mitsubishi Tanabe Pharma Corporation, Osaka, Japan) and the maxillae, including the central incisors and the titanium implants with periodontal and peri-implant tissue, were harvested. The specimens were fixed in 10% buffered formalin. The specimens were dehydrated in an ascending series of alcohol rinses and embedded in polyester resin (Rigolac 2004; Showa Highpolymer Co., Ltd., Tokyo, Japan) without decalcification. Embedded specimens were cut perpendicular to the long axis of the implants and teeth at a centerline and ground to a thickness of 100 μm with a cutting and grinding system (Maruto Instrument Co., Ltd., Tokyo, Japan). Two sections per specimen were prepared. Each section had a thickness of 30 μm, and was stained with a Villanueva–Goldner stain and observed under light microscopy.

For surface analysis of the transmucosal portion of the implants, the remaining animals were sacrificed after 8 weeks of healing using the same method as described above, and the implants were removed by inverse rotation at 20 N/cm^2 with a torque device. After removal, the implant specimens were fixed with 2.5% glutaraldehyde and dehydrated in a graded series of ethanol (50–100%). The morphology of the residual tissue at the transmucosal portion of the implant was observed under a SEM.

Eight rabbits were employed in this animal experiment. Two different types of implants placed in each rabbits. Four samples were used for each qualitative SEM and light microscopic observation of histological sections, respectively.

2.12. Nanomechanical analyses of AH-treated surface

The hardness and elastic moduli of the nanofeatured surfaces were measured using a nanoindenter (ENT-2100; Elionix Inc., Tokyo, Japan) with a Berkovich tip. The nanotopographic titanium discs were mounted on the indenter stage and pressed with the maximum load of 0.05 mN at a loading rate

Please cite this article in press as: Kato E, et al. Periodontal-like gingival connective tissue attachment on titanium surface with nano-ordered spikes and pores created by alkali-heat treatment. Dent Mater (2015), http://dx.doi.org/10.1016/j.dental.2015.01.014

of 0.1 mN/min. Subsequently, the sample was unloaded at the same rate after a 30 s pause. The indentation sites were selected under an optical microscope by a blinded technician. Indentation hardness and Young's modulus were calculated based on the established equations by ISO standards. Indentation hardness was calculated as the maximum indentation force divided by the projected area of contact computed from the load–displacement curve and the area-to-depth function. Young's modulus was calculated from the unloading segment of the load–displacement curve with an assumed Poisson ratio of 0.3.

Resistance of the nanotopographic surfaces to delamination force was evaluated by a nanoscratch test. The nanotopographic titanium discs were placed on the motorized sliding stage of the nanoscratch tester (CPX2441, Anton Paar Japan K.K., Tokyo, Japan). Scratches were generated with a spherical diamond stylus (tip radius 10 μm) at 500 mN/min at a progressive loading rate. The scratching speed was 5 mm/min. The evolution of the penetration depth, frictional force, and the friction coefficient (frictional force divided by normal force) was plotted against scratch length and force. The scratch path was subsequently observed by a light microscope equipped with the nanoscratch tester, and the point of delamination was determined. The critical load (delaminating force of the surface), defined as the minimal frictional force required for recognizable failure of the surface (*i.e.*, exposure of the titanium substrate under microscopic observation), was measured. To validate the determined delamination points, surfaces and cross-sections of the selected scratches were examined by SEM and EPMA.

The coefficient of friction and frictional resistance of AH-treated surfaces were evaluated by a nanofriction and wear test. The nanotopographic titanium discs were placed on a nanotribometer (S/N:01-105, Anton Paar Japan K.K.). Friction tracks were generated with the stainless steel ball of the tribometer by continuous lap sliding with a load of 10 mN, a lapping speed of 5 mm/s and a radius of rotation of 1 mm until the ball reached 400 laps. The profile of the coefficient of friction was plotted against the coefficient of friction and laps. The friction track was subsequently observed by a light microscope equipped with the nanotribometer, and the cross-sectional profile of the friction track was analyzed with a laser microscope (LEXT OLS4000, Olympus, Tokyo, Japan). The cross-sectional area of the wear track, defined as the worn area under the surface, was measured. Four equally spaced points across the track were measured per specimen, and the data were averaged.

For these nanomechanical analyses, three areas were measured per specimen, and the data were averaged. The set of measurements was performed in three independent specimens.

2.13. *Statistical analysis*

An analysis of variance was used to assess differences among multiple experimental groups, and when appropriate, Bonferroni multiple comparison testing was used. Student's *t*-test was used to examine differences between two groups, with a p value <0.05 considered statistically significant.

3. Result

3.1. *Nanotopographical and chemical features*

SEM images (Fig. 1A, 2000×) revealed that unidirectionally coasting waves at intervals of a few microns were observed both on the 5 and 10 M AH-treated surfaces, which was similar to the lined and wavy microgrooves on turned surfaces, but different from the micropitting structure with numerous peaks and valleys at a scale of tens of microns on the acid-etched surfaces. Higher magnification images (Fig. 1A, 10,000× and 50,000×) revealed that shaggy-like structures with many spikes and connection holes progressing to a sponge-like inner network on a nanoscale were observed on the 5 M AH-treated surface. The 10 M AH-treated surface demonstrated numerous well-organized nanoedges and spikes with many crevasses and nanoholes. The 10 M AH-treated surface was 2.5 and 1.5 times higher in number and area of nanospikes per 1 μm^2 than the 5 M AH-treated surface, respectively (Fig. 1B). The area of nanopores per 1 μm^2 was 2.5 times greater in the 5 M AH-treated surface than in the 10 M AH-treated surface. Both 5 and 10 M AH-treated surfaces had nanopores over 100 nm in diameter. The diameter was two times larger in the 10 M AH-treated surface than in the 5 M AH-treated surface.

3D isometric images under laser microscopy (Fig. 1C) demonstrated that the extent of micron asperity on the 5 and 10 M AH-treated surfaces were similar to that on the turned surface, where the asperity was formed by the turned grooves in contrast with the geometry of the acid-etched surface, which displayed over 10 micron-scaled differences in height. In terms of Ra and Rz, the 5 and 10 M AH-treated surfaces displayed values one-third of those on the acid-etched surface, and comparable with those on the turned surface (Fig. 1D). The 5 M AH-treated surface was lower in Rms value than turned and acid-etched surfaces, whereas the 10 M AH-treated surface was different in value when compared with those surfaces.

SEM and EPMA analyses for cross-sections of AH-treated surfaces demonstrated that AH treatment formed a nanostructured superficial layer containing sodium, oxygen and titanium atoms with a thickness of a few hundred nanometers on the titanium substrate, where only titanium atoms were detected (Fig. 1E). A uniform, nano-shaggy structure seemed to exist through the entire thickness of the 5 M AH-treated layer. On the other hand, the 10 M AH-treated surface seemed to exhibit closely packed bunches of finer nanoedges and spikes in the superficial portion, and a monolithic-like structure toward the titanium substrate. The nanostructured superficial layer was thicker after 10 M AH treatment (approximately 950 nm) when compared with 5 M AH treatment (approximately 600 nm) (Fig. 1F). Nanopores passed longitudinally through the entire thickness both on the 5 and 10 M AH-treated surfaces with intervals of approximately 0.5 and 1.0 μm, respectively (Fig. 1F).

3.2. *Enhanced fibroblastic attachment on nanotopographical surface*

Nuclear numbers of attached fibroblastic cells in day 1 cultures were comparable, but cell shapes were very different between

Please cite this article in press as: Kato E, et al. Periodontal-like gingival connective tissue attachment on titanium surface with nano-ordered spikes and pores created by alkali-heat treatment. Dent Mater (2015), http://dx.doi.org/10.1016/j.dental.2015.01.014

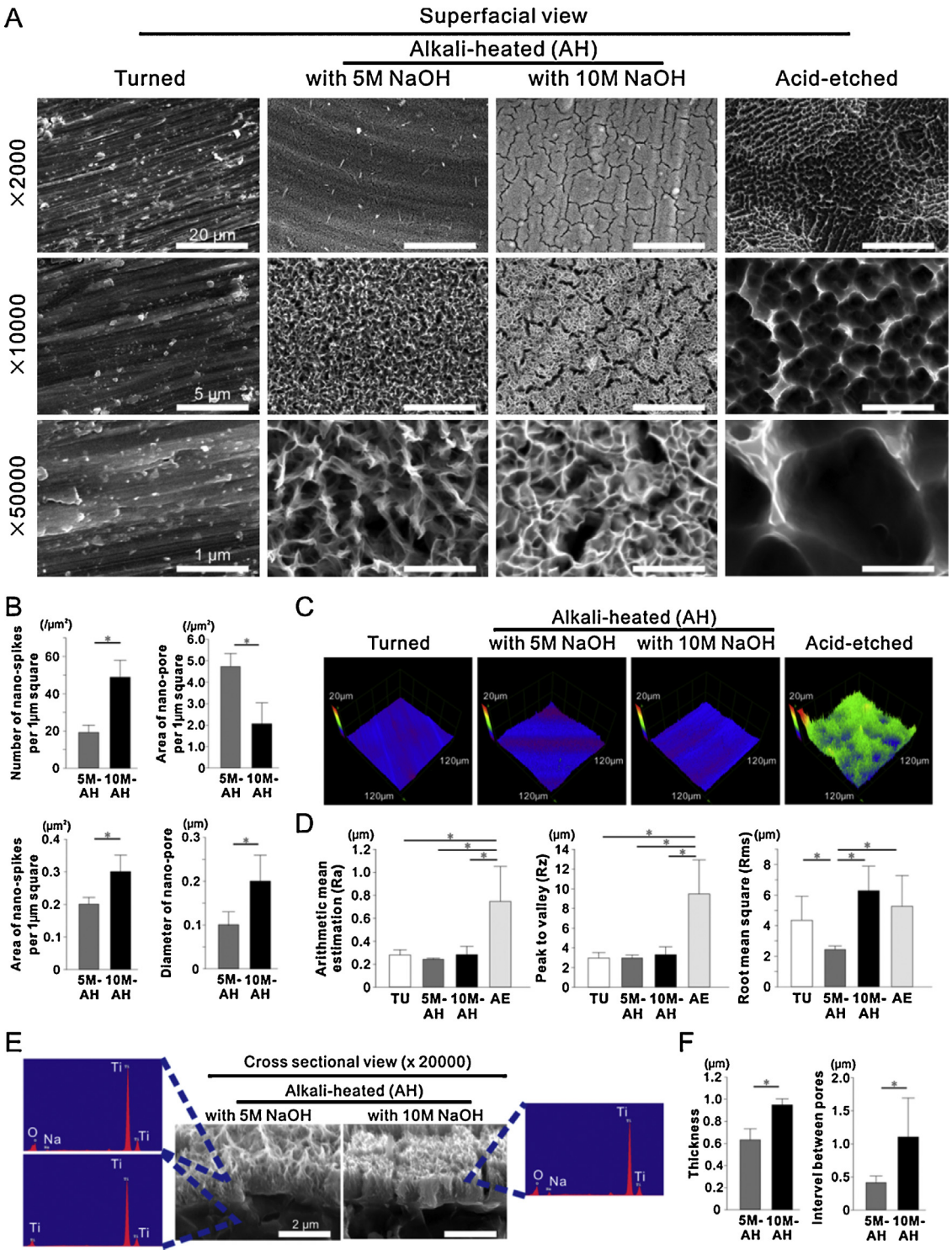

Fig. 1 – (A) Representative SEM images of titanium discs with turned, 5 and 10 M AH-treated, and acid-etched surfaces. Bar scale in images are equal within the same magnification. (B) Morphometric results based on SEM images of titanium discs with the 5 and 10 M AH-treated surfaces showing nanospikes and pores. (C) Laser microscopic 3D images and (D) quantitative measurements for three surface roughness parameters of titanium discs with turned, 5 and 10 M AH-treated, and acid-etched surfaces. (E) Representative SEM images and EPMA waveforms on cross-sections of the 5 and 10 M AH-treated surfaces on titanium films. (F) Morphometric results based on SEM images of cross-sections of the 5 and 10 M AH-treated surfaces on titanium films showing the thickness and interval between nanopores. Data represent mean ± SD ($n = 3$). $^{*}p < 0.05$, indicating a statistically significant difference between multiple experimental groups (Bonferroni) and differences between two groups (Student's t-test).

Please cite this article in press as: Kato E, et al. Periodontal-like gingival connective tissue attachment on titanium surface with nano-ordered spikes and pores created by alkali-heat treatment. Dent Mater (2015), http://dx.doi.org/10.1016/j.dental.2015.01.014

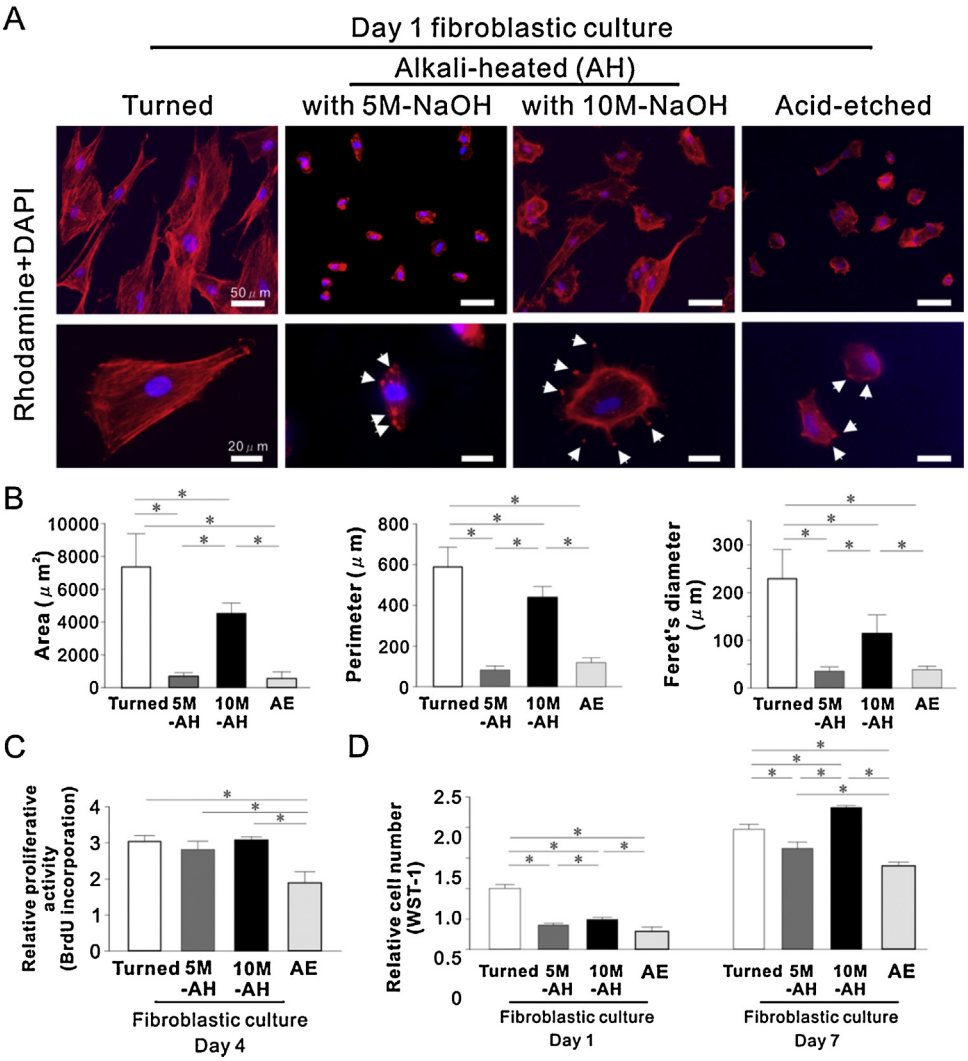

Fig. 2 – (A) Representative fluorescent photomicroscopic images after staining with rhodamine phalloidin for actin filaments (red color) and DAPI for nuclei (blue color) in day 1 fibroblastic cultures on titanium discs with turned, 5 and 10 M AH-treated, and acid-etched surfaces. (B) Cytomorphometric evaluations based on images presented in panel A. Results of proliferative activity by BrdU assay at day 4 (C) and attached cell number by WST-1 assay at days 1 and 7 (D) of fibroblastic cultures on titanium discs with turned, 5 and 10 M AH-treated, and acid-etched surfaces. Data represent mean ± SD ($n = 6$ in cytomorphometric evaluations and $n = 3$ in BrdU incorporation and WST-1 assays). *$p < 0.05$, indicating a statistically significant difference between multiple experimental groups (Bonferroni).

all surface types (Fig. 2A, upper images). Gingival fibroblasts were apparently small, but of an angular shape, with orientation in various directions on the 5 M AH-treated surface, in contrast with spindle-shaped cells with unidirectional elongation and expansion on the turned surface. Cells on the 10 M AH-treated surface exhibited multiple morphologies, including rectangular, spindle or oval shapes with moderate expansion. Cells on the acid-etched surface were small circular and rectangular shapes. Higher magnification images (Fig. 2A, lower images) demonstrated that cells on the 5 M AH-treated surface developed actin fiber formation with a uniform direction of orientation and particular areas of accumulation (arrowheads in Fig. 2A, lower images), in contrast with cells with relatively well-developed and unidirectional actin formation and lamellipodia on the turned surface. Cells on the 10 M AH-treated surface developed a cytoskeletal network with multiple orientations, multiplicity of filopodia with actin accumulation on the tips, and a contractile ring-like structure. Cells on the acid-etched surface exhibited some actin accumulation along the cellular circumference, but poor cytoskeletal arrangement. Cell morphological parameters such as area, perimeter and Feret's diameter on the acid-etched and 5 M AH-treated surfaces were less than 20% of those values on the turned surface (Fig. 2B, $p < 0.05$, Bonferroni). In contrast, these values on the 10 M AH-treated surface exceeded 50% of those on the turned surface.

3.3. *No impairment of cellular proliferation on nanotopographical surface*

Cellular proliferative activity in day 4 cultures was the lowest on the acid-etched surface and was comparable between

the turned, 5 and 10 M AH-treated surfaces (Fig. 2C) ($p > 0.05$). Relative cell numbers quantified with WST-1 on the 5 or 10 M AH-treated or acid-etched surfaces were 50% or less than those on the turned surface on day 1 (Fig. 2D) ($p < 0.05$). However, the number became greater on the 10 M AH-treated surface when compared with the turned surface on day 7 ($p < 0.05$). The number on the 5 M AH-treated surface reached 80% of that on the turned surface and greater than this on the acid-etched surface ($p < 0.05$).

3.4. *Enhanced collagen synthesis on nanotopographical surface*

The 10 M AH-treated surface consistently upregulated collagen I expression at days 7 and 14 as compared with that on the turned surface (Fig. 3A). Collagen III expression also increased on the 10 M AH-treated surface at day 7. The 5 M AH-treated surface was not much higher in collagen I expression at days 7 and 14, but was substantially higher in collagen III expression at day 7 than those on the turned surface. The acid-etched surface upregulated collagen I and III expression to levels equivalent to those on the 10 M AH-treated surface at day 7, but both expressions had disappeared at day 14, in contrast with the prolonged expression on the 10 M AH-treated surface. Sirius red staining of day 21 cultures demonstrated that collagen deposition increased by 1.3 times on the 5 and 10 M AH-treated and acid-etched surfaces as compared with that on the turned surface (Fig. 3B) ($p < 0.05$).

3.5. *Fibroblastic ECM clinging to nanotopographical surface*

SEM observation of day 21 cultures at low magnification (Fig. 3C, 2000×) demonstrated that fibroblastic ECM broadly covered any surface type. The matrix deposition was oriented along the direction of the turned grooves on the 5 and 10 M AH-treated surfaces, in contrast with the fabric-like architecture or irregular expansion on the turned or acid-etched surfaces, respectively. However, it was observed under moderate magnification (Fig. 3C, 10,000×) that the matrix seemed to be deposited but not bound to the turned surface. On one hand, fibroblastic ECM was entangled by the ridges and covered with a layer connecting the peaks on the acid-etched surface. The AH-treated surface appeared to allow the fibroblastic matrix to uniformly cover the surface without any entanglement in the projections (Fig. 3C, 10,000×). However, high magnification demonstrated that the matrix clung closely to nano-shaggy spikes or nanoedges on the 5 or 10 M AH-treated surfaces (Fig. 3C, 10,000×, arrowheads). Moreover, the matrix seemed to partially infiltrate and form a deeper connection within the inner structures of the 5 and 10 M AH-treated surfaces (Fig. 3C, 50,000×, arrowheads).

3.6. *Fibroblastic ECM infiltrating into nanotopographical surface*

SEM observation of cross-section of day 21 fibroblastic culture on the 5 M and 10 M AH-treated surface demonstrated that fibroblastic ECM covered the top of nano-structural layer (Fig. 3D, 20,000×, arrowheads). Moreover, the bottom of covered matrix appeared to come into the inside of nano-structural layer (Fig. 3D, 60,000×, arrowheads). Their border within the internal structure of the AH-treated surfaces was unclear and they looked incorporated firmly. EPMA analysis on cross-section of day 21 fibroblastic culture on the 10 M AH-treated surface demonstrated the high peaks of carbon and phosphorous were detected within the inside of surface, which was highly detected in the ECM region but not in titanium substrate (Fig. 3D, 60,000×, peak histograms). Those elements were not detected in the cross-section of surface without culture (Fig. 1E).

3.7. *Fibroblastic collagen anchoring on nanotopographical surface with reinforcements of mechanical, enzymatic and chemical strengths*

Sixty percent or more of deposited collagen still existed on the 5 and 10 M AH-treated surfaces after exposure to mechanical detachment force using ultrasonication, in contrast with 20% on the turned surface (Fig. 4A) ($p < 0.05$). The percentage of remnant collagen after exposure to collagenase, used for mimicking an inflammatory condition in cultures, was 70% and 90% in the 5 and 10 M AH-treated surfaces, respectively (Fig. 4B). These values were $1.7 - 2.0$ times higher than the value of approximately 40% on the turned surface. Over 50% of deposited collagen survived even after exposure to hydrogen peroxide, in contrast with approximately 30% on the turned surface (Fig. 4C) ($p < 0.05$). There were no significant differences in the percentages of remnant collagen after these detachment treatments between the turned and acid-etched surfaces (Fig. 4A–C) ($p > 0.05$). The 5 and 10 M AH-treated surfaces appeared to maintain deposited ECM following breakdown of the ECM by collagenase treatment, in contrast with disappearance of most of the ECM in the turned and acid-etched surfaces (Fig. 4D). In particular, most of the ECM remained deposited onto the 10 M AH-treated surface. The damaged ECM on the 5 and 10 M AH-treated surfaces extruded from the broken end as bush-like projections (Fig. 4D).

3.8. *Insertion of connective tissue into nanotopographical surface*

As was the case in culture discs, the AH-treated implant surface exhibited both an inherent microscaled wavy form at a micron level, owing to turned grooves of the turned implant substrate (Fig. 5C–E), and well-organized nanoedges and spikes with numerous crevasses and nanoholes (Fig. 5F–H). SEM observation of the transmucosal portion of turned implants placed on the palatal aspect of the upper central incisors of rabbits, and removed by inverse rotation after 8 weeks of healing, demonstrated a degree of tissue attachment on the implant surface (Fig. 5J and K, asterisks). The margin of the attached tissue on the turned surface was visually unclear (Fig. 5L, arrowheads). In contrast, abundant tissue attached to the transmucosal aspect of the implants with the nanotopographic surface (Fig. 5M, asterisks). The attached tissue on the AH-treated surface seemed to exhibit a wavy form corresponding to the groovy microgeometry of the substrate. The

Please cite this article in press as: Kato E, et al. Periodontal-like gingival connective tissue attachment on titanium surface with nano-ordered spikes and pores created by alkali-heat treatment. Dent Mater (2015), http://dx.doi.org/10.1016/j.dental.2015.01.014

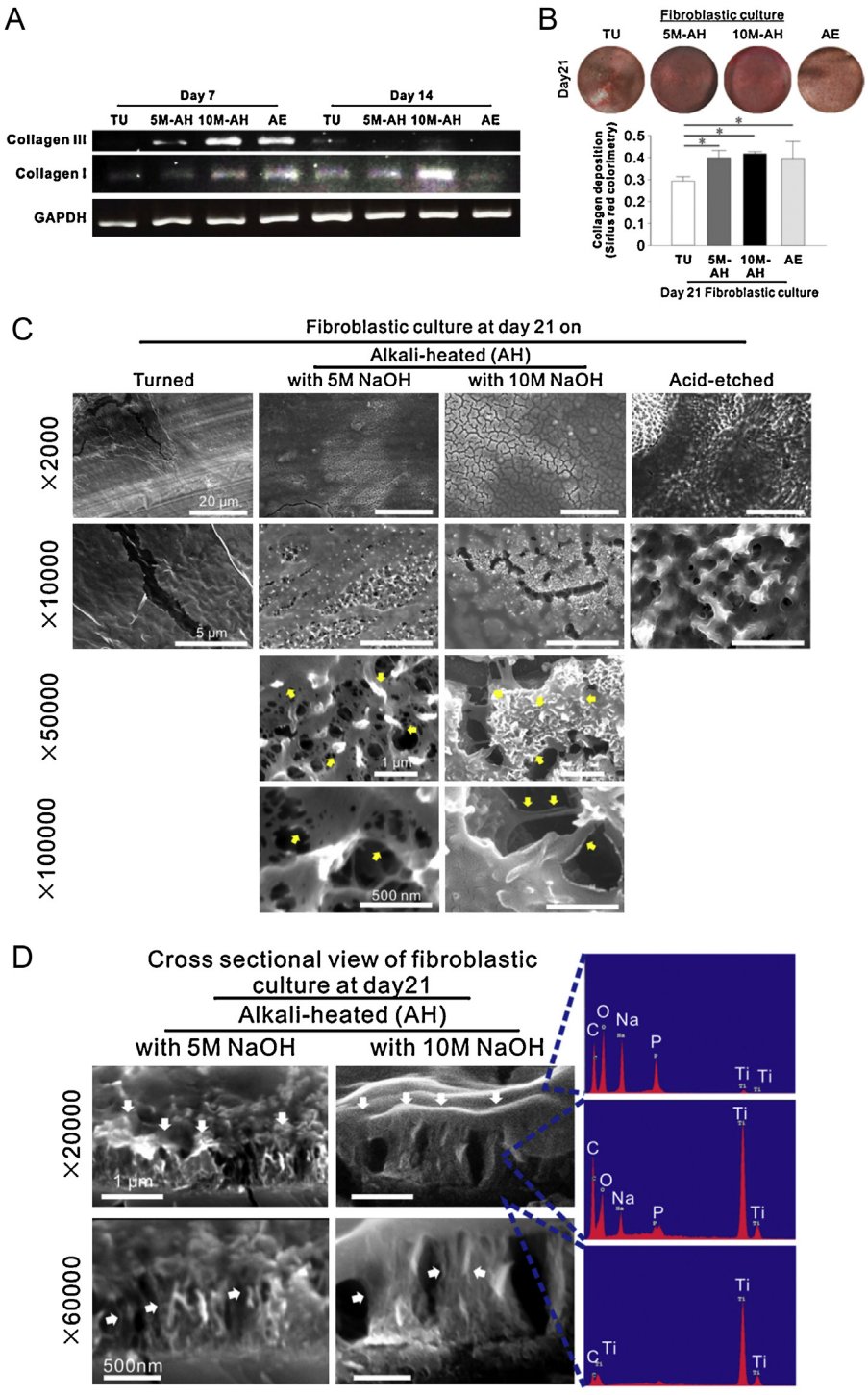

Fig. 3 – (A) Expression of collagen I and III genes analyzed by the reverse-transcriptase polymerase chain reaction method in day 7 and 14 fibroblastic cultures on titanium discs with turned, 5 and 10 M AH-treated, and acid-etched surfaces. (B) Results of collagen deposition by Sirius red staining and colorimetry in day 21 fibroblastic cultures on titanium discs with turned, 5 and 10 M AH-treated, and acid-etched surfaces. Data represent mean ± SD ($n = 3$). $^{*}p < 0.05$, indicating a statistically significant difference between multiple experimental groups (Bonferroni). Representative SEM images and EPMA waveforms of day 21 fibroblastic cultures on titanium discs with turned, 5 and 10 M AH-treated, and acid-etched surfaces (C) and cross-sections of day 21 fibroblastic cultures on titanium films with the 5 and 10 M AH-treated surfaces (D). Note that the 5 and 10 M AH-treated surfaces allow entanglement and inclusion of fibroblastic ECM with nanospikes, pores or crevasses (C) and that fibroblastic ECM extends into the inner structure of the nanotopographic layer in the 5 and 10 M AH-treated surfaces (D). Bar scale in images are equal within the same magnification.

Please cite this article in press as: Kato E, et al. Periodontal-like gingival connective tissue attachment on titanium surface with nano-ordered spikes and pores created by alkali-heat treatment. Dent Mater (2015), http://dx.doi.org/10.1016/j.dental.2015.01.014

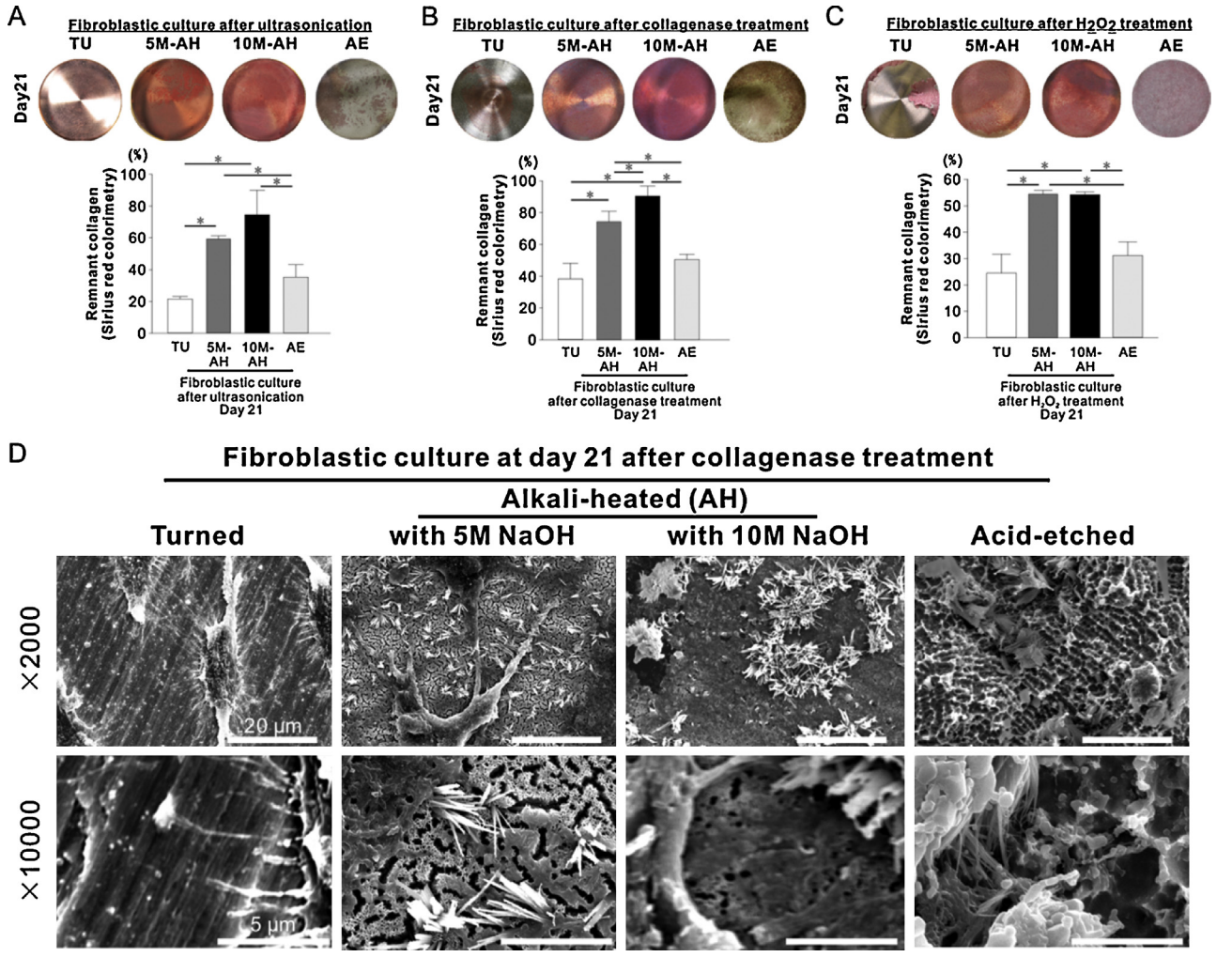

Fig. 4 – Results of remnant collagen deposition by Sirius red staining and colorimetry in day 21 fibroblastic cultures on titanium discs with turned, 5 and 10 M AH-treated, and acid-etched surfaces after ultrasonic (A), collagenase (B) or hydrogen peroxide (C) treatment. Data represent mean ± SD ($n = 3$). *$p < 0.05$, indicating a statistically significant difference between multiple experimental groups (Bonferroni). Representative SEM images of day 21 fibroblastic cultures on titanium discs with turned, 5 and 10 M AH-treated, and acid-etched surfaces after collagenase treatment (D). Bar scale in images are equal within the same magnification.

nanotopographic surface allowed termination of the attached tissue into the nanopores (Fig. 5O and P, arrowheads).

3.9. *Periodontal-like collagen fiber network on nanotopographical implant surface*

Histological sections of peri-implant tissue at the transmucosal aspect with Villanueva–Goldner staining demonstrated that the density of collagen fibers seemed poor around the turned implant surface (Fig. 6Q). The collagen fibers were directed in parallel with the surface and also ran relatively close to the surface (Fig. 6R, double-headed arrow region), becoming irregular with increasing distance from the surface (Fig. 6R, black arrowheads within a single-headed arrow region). In contrast, a dense collagen network was formed on the implants the nanotopographic surface (Fig. 6S). Abundant cells were accumulated and layered on the nanotopographic surface (Fig. 6T, double-headed arrow region). A large number of the outer collagen fibers were bundled together and oriented upward, appearing to stand from the surface (Fig. 6T, white arrowheads within a single-headed arrow region). Similar collagen networks were found in the connective tissue attachment region of the periodontal tissue (Fig. 6U and V), which consisted of a cell rich layer on cementum (Fig. 6V, double-headed arrow region) following Sharpey's fibers and the outer dentogingival (alveolar) fibers (Fig. 6V, white arrowheads within a single-headed arrow region).

3.10. *Nanomechanical property of AH-treated surface*

Nanoscratch testing demonstrated that the 5 M AH-treated surface displayed a higher delamination load than the 10 M AH-treated surface (Fig. 6A) ($p < 0.05$, Student's *t*-test). The values were 187 and 146 mN in the 5 and 10 M AH-treated surfaces, respectively. Nanoindentation testing demonstrated that the 10 M AH-treated surface was 1.3 and 1.4 times higher

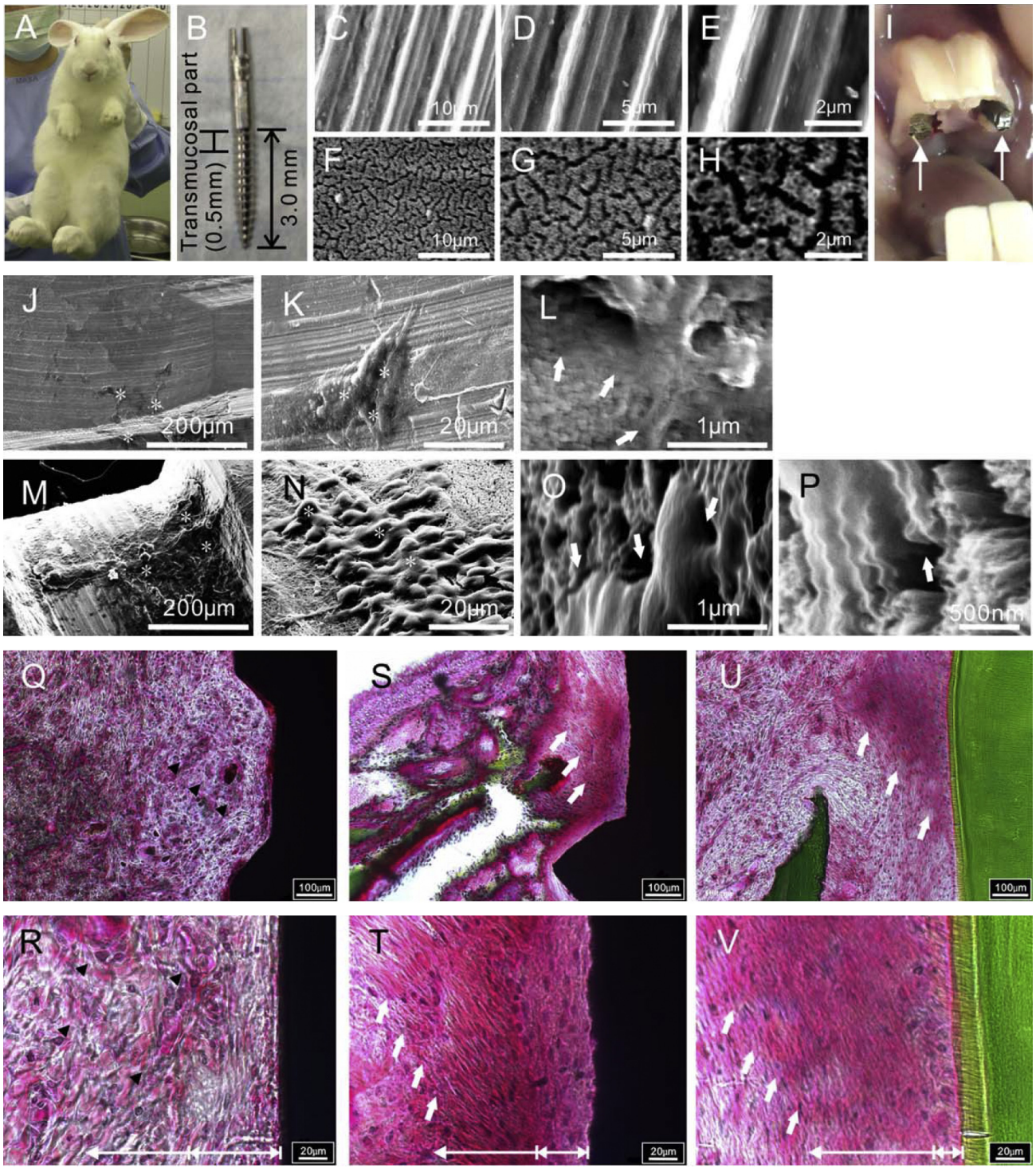

Fig. 5 – Titanium mini-implants (B) with turned (C–E) or 10 M AH-treated surfaces (F–H) were inserted into the hard palatal plate (I) of sixteen-week-old male Japanese white rabbits (A). Representative SEM images of the transmucosal aspect of implants with turned (J–L) or 10 M AH-treated surfaces (M–P) following removal by inverse rotation after 8 weeks of healing. Bar scale in images are equal within the same magnification. Asterisks indicate attached gingival tissue on the surface. Note that the gingival tissue terminates within the nanopores or crevasses on the 10 M AH-treated surface (white arrows in O and P), in contrast with the unclear margin of the attached tissue on turned implants (white arrows in L). Representative histological section with Villanueva–Goldner staining of peri-implant tissue around titanium implants with turned (Q and R) or 10 M AH-treated surfaces (S and T) at the transmucosal aspect, and the periodontal tissue of a rabbit (U and V). Note that a large number of the outer collagen fibers were bundled together to orient upward, appearing to stand from the 10 M AH-treated surface (white arrows in S and T) or tooth surface (white arrows in S and T), in contrast with the irregular collagen orientation on the turned implant surface (black arrowheads in Q and R).

Please cite this article in press as: Kato E, et al. Periodontal-like gingival connective tissue attachment on titanium surface with nano-ordered spikes and pores created by alkali-heat treatment. Dent Mater (2015), http://dx.doi.org/10.1016/j.dental.2015.01.014

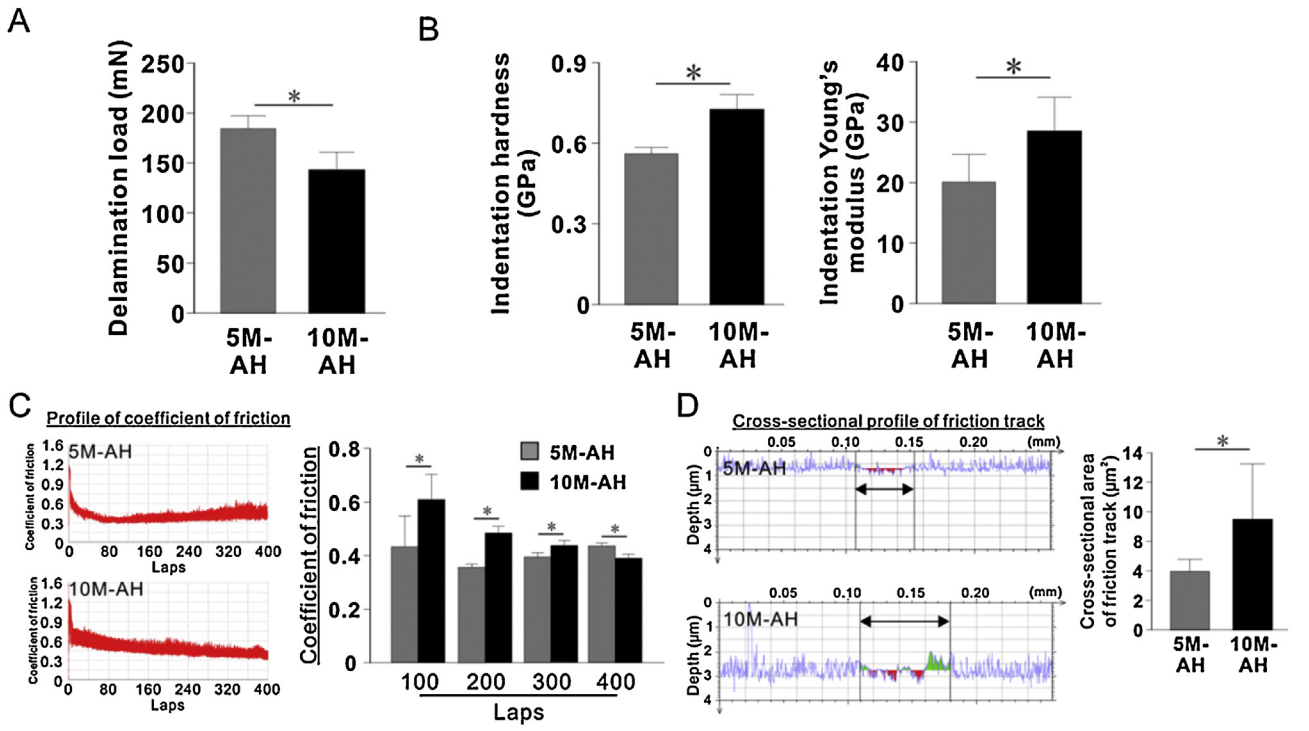

Fig. 6 – Results of delamination load from nanoscratch testing (A) and the indentation hardness and Young's modulus from nanoindentation testing (B) on the 5 and 10 M AH-treated surfaces. Profiles and results of the coefficient of friction with increasing laps (C) and the cross-sectional profiles and the area of the friction track after 400 laps (D) in nanofriction testing of the 5 and 10 M AH-treated surfaces. Data represent mean ± SD ($n = 3$). $^*p < 0.05$, indicating a statistically significant difference between two groups (Student's t-test).

in indentation hardness and Young's modulus than the 5 M AH-treated surface, respectively (Fig. 6B) ($p < 0.05$). The values were 0.56 and 0.72 GPa in indentation hardness and 20.3 and 28.6 GPa in Young's modulus on the 5 and 10 M AH-treated surfaces, respectively. The coefficient of friction by nanofriction testing was greater on the 10 M AH-treated surface than on the 5 M AH-treated surface until 300 laps, but the difference was reversed after 400 laps (Fig. 6C) ($p < 0.05$). A cross-sectional profile of the friction track appeared deeper and wider on the 10 M AH-treated surface than on the 5 M AH-treated surface (Fig. 6D, left profiles). The cross-sectional area of the friction track was over two times greater on the 10 M AH-treated surface than on the 5 M AH-treated surface (Fig. 6D, right histograms) ($p < 0.05$).

4. Discussion

Nanotopography on the 5 M AH-treated surface was characterized as porous and shaggy in structure, consisting of a greater number of nanopores with many nanospikes and a 3D internal network. The well-organized nanocrevasses progressing to a 3D internal network, with a greater number of nanospikes and edges were created on titanium surface by 10 M AH-treatment. Nanofriction testing demonstrated that the coefficient of friction on 10 M AH-treated surface was higher than that of the 5 M AH-treated surface until 300 laps and gradually reduced with increasing laps, in contrast with the consistently unchanged value on the 5 M AH-treated surface through the entire thickness. The friction track was wider and deeper on the 10 M AH-treated surface. These results supported cross-sectional morphological observation under SEM, showing closely packed bunches of finer nanoedges and spikes in the superficial aspect, with a monolithic-like structure toward the titanium substrate on the 10 M AH-treated surface, in contrast with a uniform nano-shaggy structure present through the entire thickness on the 5 M AH-treated surface.

The nanotopographic surface by AH-treatment allowed inclusion of collagen fibers into the surface with substantial reinforcement against mechanical and physicochemical detachment forces. The strength of collagen anchorage on the nanotopographic surface exceeded that on the turned or acid-etched surfaces. Deposited fibroblastic ECM was anchored with nanospikes and pores on the AH-treated surface, in contrast with layered or entangled, but not bound ECM, on the turned and acid-etched surfaces. Inclusion of gingival tissue into the nanotopographic surface was confirmed by SEM observation in a rabbit maxilla model using mini-implants. These findings display the first evidence that connective tissue collagen fiber attachment similar to periodontal Sharpey's fibers could be achieved on the nanotopographic titanium surface. Application of the nanotopographic process for the transmucosal aspect of dental titanium implants may improve clinical stability of peri-implant tissue as compared with that around conventional surface topographies, such as smooth and microroughened surfaces.

The strength of collagen anchorage on the 10 M AH-treated surface rivaled or surpassed that on the 5 M AH-treated

Please cite this article in press as: Kato E, et al. Periodontal-like gingival connective tissue attachment on titanium surface with nano-ordered spikes and pores created by alkali-heat treatment. Dent Mater (2015), http://dx.doi.org/10.1016/j.dental.2015.01.014

surface in this detachment culture assay, simulating mechanical overloading and an inflammatory condition. The manner of collagen fiber binding to the nanotopographic titanium surface by the AH-treatment was characterized by entrapment of the collagen fibers with numerous nanospikes and pores or crevasses. The number of nanospikes was greater on the 10 M AH-treated surface than on the 5 M AH-treated surface. Despite greater areas of nanopores on the 5 M AH-treated surface, the diameter of the nanopores was wider on the 10 M AH-treated surface. The 10 M AH-treated surface may have an advantage over the 5 M AH-treated surface in terms of binding strength of the connective tissue, as a result of the enhanced entanglement and inclusion of larger collagen bundles.

Aside from the establishment of gingival connective tissue binding, the nanotopographic surface by the AH-treatment enhanced gingival fibroblastic collagen synthesis without deterioration of cellular proliferation. The nanotopographic or acid-etched surfaces enhanced and/or accelerated gene expression and synthesis of collagen I and III in gingival fibroblasts, as compared with those on the turned surface. The 10 M AH-treated nanotopographic surface upregulated these gene expressions more than the 5 M AH-treated surface, in addition to exhibiting a higher number of nanospikes on the surface. Furthermore, fibroblastic cells on the nanotopographic surface developed a cytoskeletal network and punctate accumulations by actin fibers, in contrast with little accumulation or cytoskeletal arrangement on the turned or acid-etched surfaces. The cell shapes on the nanotopographic surface were smaller than on the turned surface, but appeared angular or rectangular. In particular, the 10 M AH-treated nanotopographic surface also allowed fibroblasts to develop multiple filopodia-like cellular projections with expansion of the cell body. This indicates that the nanotopographic surface promoted formation of focal adhesion plaques and cytoskeletal arrangement. Nanotopography can interact with cell membrane receptors such as integrin which connects to adaptor and cytoskeletal proteins. Focal adhesion plaques consist of these adhesion, adaptor and cytoskeletal proteins. The plaques capture and integrate various signals from both the extracellular and intracellular environments [36,37], and initiate a cellular signaling pathway to regulate the formation of cellular projections and the cytoskeletal actin fiber network [38,39], which results in the coordinated controls of fundamental cellular processes such as differentiation, cell cycle control, apoptosis and motility [36,40]. It is known that ordered nanofeatures on a substrate can govern various types of cell differentiation, including endothelial cells, osteoblasts, fibroblasts and mesenchymal or embryonic stem cells [18,41–44]. The nanotopographic, in particular the 10 M AH-treated, surface may enhance the ECM production capability of fibroblasts through activation of cellular signaling related to focal adhesion plaques with numerous nanospikes on the surface.

Nanoindentation testing on the AH-treated nanotopographic surface demonstrated 0.56 or 0.72 GPa in indentation hardness and 20.3 or 28.6 GPa in Young's modulus on the 5 or 10 M AH-treated surfaces, respectively. These values rivaled or surpassed the values of human cementum, dentin and alveolar bone, which was determined by nanoindentation [45–48]. Again, the nanotopographic surface, in particular the 10 M AH-treated surface, allowed development of filopodia-like cellular projections of attached gingival fibroblasts and intrusion of fibroblastic ECM into the surface. Intrusion of ECM into the surface may require invasion of cellular projections into the inner aspect of the nanotopographic layer. Filopodia are cellular sensors for various substrate features, such as stiffness [49] or nanotopography [50]. The influence of the mechanical and physicochemical properties of the nanotopographic titanium surface by AH-treatment on fibroblastic cellular sensing systems as the mechanism underlying establishment of intrusion of ECM into the surface would be of great interest for future research.

Delamination of the superficial layer of the substrate after functional loading is one of the important issues of load-bearing devices. By the same token in natural teeth, cementum on the tooth root sometimes suffers from cemental tears caused by excessive occlusal loading [51]. Nanoscratch testing was able to evaluate the mechanical strength between the nanotopographic layer and the titanium substrate. In this study, the delamination load between the nanotopographic layer and the titanium substrate was 187 and 146 mN in the 5 and 10 M AH-treated surfaces, respectively. Although there was no information in previous literature about delamination load at the cementum–dentin junction, these values were much higher than the values of mineralized ECM–titanium interface in osteoblastic cell cultures on various titanium surfaces [52–54]. In addition, the thickness of the nanotopographic layer on the AH-treated surface was under 1.0 μm (approximately, 600 nm and 950 nm on the 5 and 10 M AH-treated surfaces, respectively), in contrast with several dozen to hundreds of micrometers in thickness of cementum. A nano-ordered, thin coating on implants is known to be effective in preventing delamination between the coating layer and substrate [55,56]. When considered in conjunction with indentation hardness and Young's modulus, it was estimated that the nanotopographic surface by the AH-treatment had substantial mechanical strength for application on the transmucosal aspect of dental implants.

The connective tissue layer on the transmucosal aspect of titanium implants (traditionally with a turned or machined titanium surface) is generally divided into two zones. The inner zone, which directly contacts the surface of the transmucosal component, is a scar-like fibroblast-poor layer with 50 – 100 μm thickness [10,12,57–60]. The remaining connective tissue, the outer zone, is formed of fibers running in different directions with abundant fibroblasts and blood vessels [10]. In this study, the 10 M AH-treated nanotopographic surface facilitated inclusion of gingival collagen fibers into the surface, similar to Sharpey's fibers. More interestingly, the surface yielded a gingival collagen fiber orientation similar to dentogingival fibers in periodontal tissue, despite no such certain microtopographical features. Orientation of periodontal connective tissue fibers is expected to follow sequential formation of Sharpey's fibers and cementogenesis during tooth eruption. Therefore, it was assumed that the nanotopography initiated an algorithm similar to the formation of dentogingival fibers, by inclusion of collagen fibers, and achieved the formation of a peri-implant connective tissue layer mimicking periodontal connective tissue. Further investigations would be required to clarify this interesting assumption.

Please cite this article in press as: Kato E, et al. Periodontal-like gingival connective tissue attachment on titanium surface with nano-ordered spikes and pores created by alkali-heat treatment. Dent Mater (2015), http://dx.doi.org/10.1016/j.dental.2015.01.014

5. Conclusion

The nanotopographic titanium surface created by AH-treatment exhibited numerous well-organized nanoedges and spikes, crevasses and nanoholes or the uniform shaggy-like nanotopography and sponge-like inner network. The nanotopographic titanium surface with nanoedges, spikes and crevasses enhanced gingival fibroblastic cellular adhesion and collagen synthesis, and toughened binding strength of deposited collagen enough to resist against experimental overloading and inflammatory conditions by inclusion of collagen fibers into the surface. The inclusion of gingival connective tissue into the surface, with arrangement of collagen fiber directions mimicking periodontal tissue, was confirmed in a rabbit maxilla model.

Conflict of interest

All authors have no conflicts of interest.

Acknowledgments

The author would like to thank research associate Eiko Watanabe of the Oral Health Science Center for her assistance with the evaluation of chemical composition by EPMA. This research was supported by Grant-in-Aid for Scientific Research (C) of Japan, 2014–2016 (grant number 26462978).

REFERENCES

[1] Berglundh T, Lindhe J, Ericsson I, Marinello CP, Liljenberg B, Thomsen P. The soft tissue barrier at implants and teeth. Clin Oral Implants Res 1991;2:81–90.
[2] Rompen E, Domken O, Degidi M, Pontes AE, Piattelli A. The effect of material characteristics, of surface topography and of implant components and connections on soft tissue integration: a literature review. Clin Oral Implants Res 2006;17(Suppl. 2):55–67.
[3] Gargiulo AW, Wentz FM, Orban B. Mitotic activity of human oral epithelium exposed to 30 per cent hydrogen peroxide. Oral Surg Oral Med Oral Pathol 1961;14:474–92.
[4] Stern IB. Current concepts of the dentogingival junction: the epithelial and connective tissue attachments to the tooth. J Periodontol 1981;52:465–76.
[5] Nevins M, Nevins ML, Camelo M, Boyesen JL, Kim DM. Human histologic evidence of a connective tissue attachment to a dental implant. Int J Periodontics Restor Dent 2008;28:111–21.
[6] Nevins M, Kim DM, Jun SH, Guze K, Schupbach P, Nevins ML. Histologic evidence of a connective tissue attachment to laser microgrooved abutments: a canine study. Int J Periodontics Restor Dent 2010;30:245–55.
[7] Shin SY, Han DH. Influence of a microgrooved collar design on soft and hard tissue healing of immediate implantation in fresh extraction sites in dogs. Clin Oral Implants Res 2010;21:804–14.
[8] Schroeder A, van der Zypen E, Stich H, Sutter F. The reactions of bone, connective tissue, and epithelium to endosteal implants with titanium-sprayed surfaces. J Maxillofac Surg 1981;9:15–25.
[9] Deporter DA, Watson PA, Pilliar RM, Howley TP, Winslow J. A histological evaluation of a functional endosseous, porous-surfaced, titanium alloy dental implant system in the dog. J Den Res 1988;67:1190–5.
[10] Buser D, Weber HP, Donath K, Fiorellini JP, Paquette DW, Williams RC. Soft tissue reactions to non-submerged unloaded titanium implants in beagle dogs. J Periodontol 1992;63:225–35.
[11] Listgarten MA, Buser D, Steinemann SG, Donath K, Lang NP, Weber HP. Light and transmission electron microscopy of the intact interfaces between non-submerged titanium-coated epoxy resin implants and bone or gingiva. J Dent Res 1992;71:364–71.
[12] Chavrier C, Couble ML, Hartmann DJ. Qualitative study of collagenous and noncollagenous glycoproteins of the human healthy keratinized mucosa surrounding implants. Clin Oral Implants Res 1994;5:117–24.
[13] Jiang H, Grinnell F. Cell-matrix entanglement and mechanical anchorage of fibroblasts in three-dimensional collagen matrices. Mol Biol Cell 2005;16:5070–6.
[14] Kubo K, Tsukimura N, Iwasa F, Ueno T, Saruwatari L, Aita H, et al. Cellular behavior on TiO_2 nanonodular structures in a micro-to-nanoscale hierarchy model. Biomaterials 2009;30:5319–29.
[15] Raimondo T, Puckett S, Webster TJ. Greater osteoblast and endothelial cell adhesion on nanostructured polyethylene and titanium. Int J Nanomed 2010;5:647–52.
[16] Yao C, Slamovich EB, Webster TJ. Enhanced osteoblast functions on anodized titanium with nanotube-like structures. J Biomed Mater Res A 2008;85:157–66.
[17] Ballo A, Agheli H, Lausmaa J, Thomsen P, Petronis S. Nanostructured model implants for in vivo studies: influence of well-defined nanotopography on de novo bone formation on titanium implants. Int J Nanomed 2011;6:3415–28.
[18] Mendonca G, Mendonca DB, Aragao FJ, Cooper LF. Advancing dental implant surface technology – from micron- to nanotopography. Biomaterials 2008;29:3822–35.
[19] Divya Rani VV, Manzoor K, Menon D, Selvamurugan N, Nair SV. The design of novel nanostructures on titanium by solution chemistry for an improved osteoblast response. Nanotechnology 2009;20:195101.
[20] Cooper LF, Zhou Y, Takebe J, Guo J, Abron A, Holmen A, et al. Fluoride modification effects on osteoblast behavior and bone formation at TiO_2 grit-blasted c.p. titanium endosseous implants. Biomaterials 2006;27:926–36.
[21] Ellingsen JE, Johansson CB, Wennerberg A, Holmen A. Improved retention and bone-tolmplant contact with fluoride-modified titanium implants. Int J Oral Maxillofac Implants 2004;19:659–66.
[22] Salasznyk RM, Klees RF, Williams WA, Boskey A, Plopper GE. Focal adhesion kinase signaling pathways regulate the osteogenic differentiation of human mesenchymal stem cells. Exp Cell Res 2007;313:22–37.
[23] Mathieu PS, Loboa EG. Cytoskeletal and focal adhesion influences on mesenchymal stem cell shape, mechanical properties, and differentiation down osteogenic, adipogenic, and chondrogenic pathways. Tissue Eng B: Rev 2012;18:436–44.
[24] Abarrategi A, Gutierrez MC, Moreno-Vicente C, Hortiguela MJ, Ramos V, Lopez-Lacomba JL, et al. Multiwall carbon nanotube scaffolds for tissue engineering purposes. Biomaterials 2008;29:94–102.
[25] Usui Y, Aoki K, Narita N, Murakami N, Nakamura I, Nakamura K, et al. Carbon nanotubes with high bone-tissue compatibility and bone-formation acceleration effects. Small 2008;4:240–6.

Please cite this article in press as: Kato E, et al. Periodontal-like gingival connective tissue attachment on titanium surface with nano-ordered spikes and pores created by alkali-heat treatment. Dent Mater (2015), http://dx.doi.org/10.1016/j.dental.2015.01.014

[26] Ueno T, Tsukimura N, Yamada M, Ogawa T. Enhanced bone-integration capability of alkali- and heat-treated nanopolymorphic titanium in micro-to-nanoscale hierarchy. Biomaterials 2011;32:7297–308.
[27] Nishio K, Neo M, Akiyama H, Nishiguchi S, Kim HM, Kokubo T, et al. The effect of alkali- and heat-treated titanium and apatite-formed titanium on osteoblastic differentiation of bone marrow cells. J Biomed Mater Res 2000;52:652–61.
[28] Kim HM, Miyaji F, Kokubo T, Nakamura T. Preparation of bioactive Ti and its alloys via simple chemical surface treatment. J Biomed Mater Res 1996;32:409–17.
[29] Miyaza T, Kim HM, Kokubo T, Ohtsuki C, Kato H, Nakamura T. Mechanism of bonelike apatite formation on bioactive tantalum metal in a simulated body fluid. Biomaterials 2002;23:827–32.
[30] Muramatsu K, Uchida M, Kim HM, Fujisawa A, Kokubo T. Thromboresistance of alkali- and heat-treated titanium metal formed with apatite. J Biomed Mater Res A 2003;65:409–16.
[31] Kubo K, Att W, Yamada M, Ohmi K, Tsukimura N, Suzuki T, et al. Microtopography of titanium suppresses osteoblastic differentiation but enhances chondroblastic differentiation of rat femoral periosteum-derived cells. J Biomed Mater Res A 2008;87:380–91.
[32] Nishiguchi S, Fujibayashi S, Kim HM, Kokubo T, Nakamura T. Biology of alkali- and heat-treated titanium implants. J Biomed Mater Res A 2003;67:26–35.
[33] Sato N, Ueno T, Kubo K, Suzuki T, Tsukimura N, Att W, et al. N-acetyl cysteine (NAC) inhibits proliferation, collagen gene transcription, and redox stress in rat palatal mucosal cells. Dent Mater 2009;25:1532–40.
[34] Att W, Yamada M, Kojima N, Ogawa T. N-acetyl cysteine prevents suppression of oral fibroblast function on poly(methylmethacrylate) resin. Acta Biomater 2009;5:391–8.
[35] Sculean A, Gruber R, Bosshardt DD. Soft tissue wound healing around teeth and dental implants. J Clin Periodontol 2014;41(Suppl. 15):S6–22.
[36] Ruoslahti E, Obrink B. Common principles in cell adhesion. Exp Cell Res 1996;227:1–11.
[37] Rosales C, O'Brien V, Kornberg L, Juliano R. Signal transduction by cell adhesion receptors. Biochim Biophys Acta 1995;1242:77–98.
[38] Tang DD, Anfinogenova Y. Physiologic properties and regulation of the actin cytoskeleton in vascular smooth muscle. J Cardiovasc Pharmacol Ther 2008;13:130–40.
[39] Chen GC, Turano B, Ruest PJ, Hagel M, Settleman J, Thomas SM. Regulation of Rho and Rac signaling to the actin cytoskeleton by paxillin during *Drosophila* development. Mol Cell Biol 2005;25:979–87.
[40] Huang S, Ingber DE. Shape-dependent control of cell growth, differentiation, and apoptosis: switching between attractors in cell regulatory networks. Exp Cell Res 2000;261:91–103.
[41] Teo BK, Wong ST, Lim CK, Kung TY, Yap CH, Ramagopal Y, et al. Nanotopography modulates mechanotransduction of stem cells and induces differentiation through focal adhesion kinase. ACS Nano 2013;7:4785–98.
[42] Dreier B, Gasiorowski JZ, Morgan JT, Nealey PF, Russell P, Murphy CJ. Early responses of vascular endothelial cells to topographic cues. Am J Physiol Cell Physiol 2013;305:C290–8.
[43] Padmanabhan J, Kinser ER, Stalter MA, Duncan-Lewis C, Balestrini JL, Sawyer AJ, et al. Engineering cellular response using nanopatterned bulk metallic glass. ACS Nano 2014;8:4366–75.
[44] Lyu Z, Wang H, Wang Y, Ding K, Liu H, Yuan L, et al. Maintaining the pluripotency of mouse embryonic stem cells on gold nanoparticle layers with nanoscale but not microscale surface roughness. Nanoscale 2014;6:6959–69.
[45] Ho SP, Balooch M, Marshall SJ, Marshall GW. Local properties of a functionally graded interphase between cementum and dentin. J Biomed Mater Res A 2004;70:480–9.
[46] Ho SP, Senkyrikova P, Marshall GW, Yun W, Wang Y, Karan K, et al. Structure, chemical composition and mechanical properties of coronal cementum in human deciduous molars. Dent Mater 2009;25:1195–204.
[47] Ho SP, Kurylo MP, Fong TK, Lee SS, Wagner HD, Ryder MI, et al. The biomechanical characteristics of the bone-periodontal ligament–cementum complex. Biomaterials 2010;31:6635–46.
[48] Ho SP, Yu B, Yun W, Marshall GW, Ryder MI, Marshall SJ. Structure, chemical composition and mechanical properties of human and rat cementum and its interface with root dentin. Acta Biomater 2009;5:707–18.
[49] Liou YR, Torng W, Kao YC, Sung KB, Lee CH, Kuo PL. Substrate stiffness regulates filopodial activities in lung cancer cells. PLoS ONE 2014;9:e89767.
[50] Albuschies J, Vogel V. The role of filopodia in the recognition of nanotopographies. Sci Rep 2013;3:1658.
[51] Stewart ML, McClanahan SB. Cemental tear: a case report. Int Endod J 2006;39:81–6.
[52] Butz F, Aita H, Takeuchi K, Ogawa T. Enhanced mineralized tissue adhesion to titanium over polystyrene assessed by the nano-scratch test. J Biomed Mater Res A 2005;74:164–70.
[53] Nakamura HK, Butz F, Saruwatari L, Ogawa T. A role for proteoglycans in mineralized tissue–titanium adhesion. J Dent Res 2007;86:147–52.
[54] Saruwatari L, Aita H, Butz F, Nakamura HK, Ouyang J, Yang Y, et al. Osteoblasts generate harder, stiffer, and more delamination-resistant mineralized tissue on titanium than on polystyrene, associated with distinct tissue micro- and ultrastructure. J Bone Miner Res 2005;20:2002–16.
[55] Nichols HL, Zhang N, Zhang J, Shi D, Bhaduri S, Wen X. Coating nanothickness degradable films on nanocrystalline hydroxyapatite particles to improve the bonding strength between nanohydroxyapatite and degradable polymer matrix. J Biomed Mater Res A 2007;82:373–82.
[56] Yang L, Sheldon BW, Webster TJ. Orthopedic nano diamond coatings: control of surface properties and their impact on osteoblast adhesion and proliferation. J Biomed Mater Res A 2009;91:548–56.
[57] Berglundh T, Lindhe J, Jonsson K, Ericsson I. The topography of the vascular systems in the periodontal and peri-implant tissues in the dog. J Clin Periodontol 1994;21:189–93.
[58] Abrahamsson I, Berglundh T, Wennstrom J, Lindhe J. The peri-implant hard and soft tissues at different implant systems. A comparative study in the dog. Clin Oral Implants Res 1996;7:212–9.
[59] Cochran DL, Hermann JS, Schenk RK, Higginbottom FL, Buser D. Biologic width around titanium implants. A histometric analysis of the implanto-gingival junction around unloaded and loaded nonsubmerged implants in the canine mandible. J Periodontol 1997;68:186–98.
[60] Schierano G, Ramieri G, Cortese M, Aimetti M, Preti G. Organization of the connective tissue barrier around long-term loaded implant abutments in man. Clin Oral Implants Res 2002;13:460–4.

Please cite this article in press as: Kato E, et al. Periodontal-like gingival connective tissue attachment on titanium surface with nano-ordered spikes and pores created by alkali-heat treatment. Dent Mater (2015), http://dx.doi.org/10.1016/j.dental.2015.01.014